IEEE Access
Multidisciplinary | Rapid Review | Open Access Journal

Received 7 June 2023, accepted 4 July 2023, date of publication 10 July 2023, date of current version 14 July 2023.

Digital Object Identifier 10.1109/ACCESS.2023.3293425

RESEARCH ARTICLE

Broadband SLMBA Design Including 90° Hybrid Frequency Response Using an Automatic Methodology

CATARINA BELCHIOR, (Graduate Student Member, IEEE), LUÍS C. NUNES, (Member, IEEE), PEDRO M. CABRAL, (Senior Member, IEEE), AND JOSÉ C. PEDRO, (Fellow, IEEE)

Departamento de Eletrónica, Telecomunicações e Informática (DETI), Instituto de Telecomunicações, Universidade de Aveiro, Campus Universitário de Santiago, 3810-193 Aveiro, Portugal

Corresponding author: Catarina Belchior (c.belchior@ua.pt)

The work of Catarina Belchior was supported in part by the Fundação para a Ciência e a Tecnologia (FCT) through Fundo Social Europeu (FSE) and in part by Programa Operacional Regional do Centro under Ph.D. work under Grant SFRH/BD/05414/2020.

ABSTRACT This article proposes an automatic methodology for the design of a sequential load-modulated balanced amplifier (SLMBA), which takes corrections for its output combiner's (a 90° hybrid) frequency response. The method uses a properly selected control amplifier phase to compensate for the 90° hybrid frequency response and finds the accurate impedances that are observed towards the hybrid. Based on this, and on a multi-dimensional search performed over the control and balanced devices' load-pull data, the optimum termination impedance profiles are found, considering the desired output power levels and efficiency. The balanced power amplifiers off-state impedance is also incorporated in the methodology to prevent the otherwise unavoidable SLMBA performance degradation. Consequently, three scattering parameter matrices are obtained in a polynomial form, corresponding to the output matching networks of the balanced and control amplifiers, and the required post-matching network at the 50 Ω output port. Finally, the method is validated with a practical SLMBA implementation, synthesizing real matching networks that realize the derived S-parameter matrices.

INDEX TERMS Automatic design, broadband matching, optimum impedance profile, power amplifier, sequential LMBA.

I. INTRODUCTION

Modern wireless communications systems rely on high peak to average power ratio (PAPR) modulated signals to meet the ever-increasing demands on higher data rates. Furthermore, since todays' communication standards operate at different center frequencies, wideband transmitters and receivers are needed, so that cost, space and system complexity can be minimized. These requirements create a strong demand for radio frequency power amplifiers (PAs) capable of providing efficient operation in an extensive range of output power levels and over a wide bandwidth.

To meet these demands, several load modulation architectures have been developed, such as the Doherty Amplifier (DPA) [1], [2], [3], [4], [5], [6], the Outphasing Amplifier [7], [8], [9], [10], [11] or the Load Modulated Balanced Amplifier (LMBA) [12], [13], [14], [15], [16], [17], [18], [19], [20]. In particular, the LMBA has been demonstrated to be an effective architecture for efficiency enhancement for high output back-off (OBO).

In its initial configuration, the load impedance of the balanced power amplifiers (BPAs) – acting as main amplifiers, biased in class B – is controlled by the amplitude and phase variations of the signal produced by the control power amplifier (CPA) – acting as an auxiliary power amplifier biased in class C – injected into the isolated port of the 90° hybrid, achieving a ''Doherty-like'' load modulation [12],

The associate editor coordinating the review of this manuscript and approving it for publication was Liang-Bi Chen.

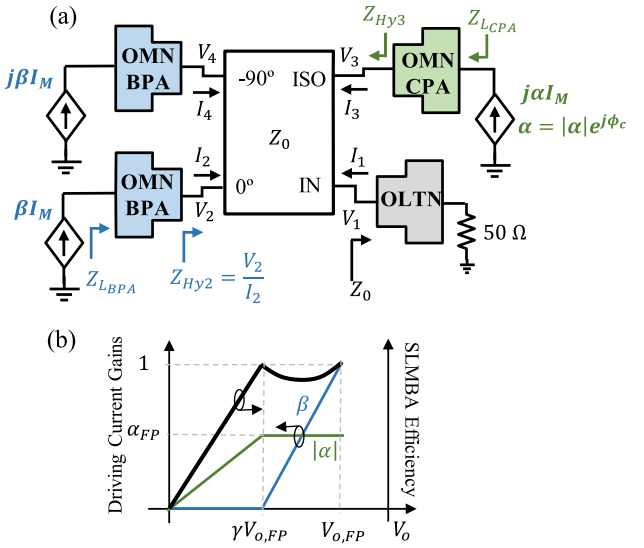

FIGURE 1. (a) Output combiner of the SLMBA composed by output matching networks (OMN) of the balanced and control devices and the output load transformer network (OLTN), (b) normalized BPAs and CPA driving signals and SLMBA efficiency.

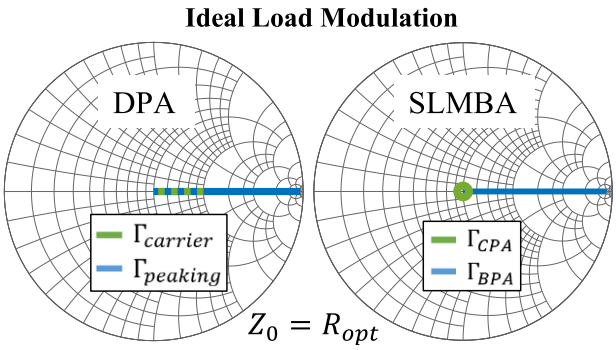

FIGURE 2. DPA and SLMBA load modulation.

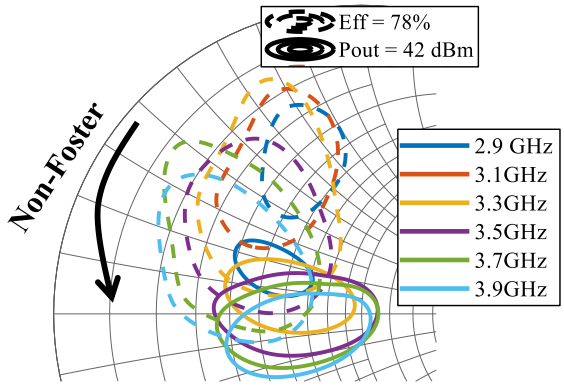

FIGURE 3. Load-pull data of a 16-W GaN-HEMT package device, demonstrating the non-Foster trajectory. Solid lines correspond to the contours with constant output power equal to 42 dBm and the dashed line to the contours with efficiency equal to 78%.

[13], [14], [15]. By reversing the operation role of the BPAs and CPA, it is possible to extend the bandwidth and power back-off range [16], [17], [18], [19], [20]. This configuration is known as sequential LMBA (SLMBA), and it is presented in Fig. 1(a). The driving current gains for the CPA and BPAs, α and β, and the SLMBA efficiency are presented in Fig.1 (b), in which γ is the normalized voltage amplitude (with respect to the full power output voltage excursion, $V_{o,FP}$) where the first efficiency peak occurs.

For low output power (P_{out}) levels, i.e., for $P_{out} < \gamma^2 P_{FP}$, only the CPA is active. The BPAs will only operate in the "load-modulation" region ($P_{out} \geq \gamma^2 P_{FP}$). The CPA is connected to the 90° hybrid coupler's isolated port, and so, ideally, the impedance presented to the CPA is kept constant across all power levels, and only the BPAs' load is dynamically changed until the full power load is reached. This operation reveals that, theoretically, the BPAs' and the CPA's OMNs only need to satisfy one load condition [17], making the wideband design more straightforward. This is demonstrated in Fig. 2, where the ideal load modulation (there is only modulation for the BPAs) of the SLMBA and its comparison with the DPA (load modulation occurs for the carrier and peaking PAs) is presented.

In practice, the PA design process starts with the power transistors choice, followed by a careful selection of their optimum impedances, considering the required design targets, such as output power and efficiency, over a specific bandwidth. The selection of these impedances is normally performed by using the measured/simulated load- and source-pull data for each carrier frequency within the required bandwidth.

Looking at the efficiency and output power contours on the Smith chart, it is easy to choose the impedance profile over frequency that leads to a certain output power and efficiency.

However, for wideband designs, this selection is not a straightforward task, even for experienced PA designers, since these optimum terminations usually follow a non-Foster trajectory, as depicted in Fig. 3, which means that these desired impedances cannot be synthesized using a passive matching network. Naturally, this task is even more difficult when harmonic terminations are considered, which, depending on the device, can significantly impact the performance.

This problem was already addressed in [21], using an automatic methodology to design the input and output matching networks (IMNs and OMNs, respectively) based on efficiency, gain and output power performance metrics. However, in that work only single-ended configurations were considered.

When complex architectures are used, such as the SLMBA, the interactions between devices need to be considered, which, added to the previously mentioned issues for the single-ended PAs, makes the matching networks (MNs) design very challenging.

In this regard, [22] and [23] proposed an automatically methodology to design an output combiner of a dual-input Doherty PA, from the current source reference plane of the transistor. Naturally, this requires an "open" nonlinear transistor model, i.e., one in which all voltage nodes are accessible, which many times is not provided by the vendors (i.e., we only have access to the package reference plane).

Alternatively, in [24] and [25] the PA MNs are directly optimized based on the desired performance metrics using a nonlinear model and electronic design automation (EDA) software. Unfortunately, this solution may fail to converge or find a satisfactory result, especially when a large number of variables with a very wide dynamic range are considered and when several goals are set. To circumvent the non-convergence issue, [26] and [27] propose a PA design method based on annealing particle swarm optimization algorithm, in which they are able to remove the "unstable" particles from the particle swarm, allowing the efficiency and output power calculations through a harmonic balance simulator. Nevertheless, besides a high complexity of the system, this solution can be very time-consuming and simulation intensive.

In [28] the methodology of [21], initially conceived for single-ended amplifiers, was extended to a state-of-the-art load-modulated PA configuration, the SLMBA, by automatically selecting the optimum impedance profiles for the output combiner design. Then, in [29], the BPA's non-infinite off-state impedance was included in the automatic design methodology.

In this paper, this automatic design methodology is taken one step further, by incorporating the non-ideal 90° hybrid coupler, and thus correcting its detrimental effect on the PA performance. A comprehensive objective function is given, considering the imperfect isolation and the phase imbalance of the hybrid and also the desired second harmonic impedance profile, this way improving the bandwidth achievable with the developed automated PA design methodology.

Based on load-pull data and on a pre-designed 90° hybrid, the optimum impedance profiles for the load combiner design are automatically selected, considering fundamental and harmonic terminations. Therefore, the proposed automatic methodology does not require an "open" device model or the use of nonlinear optimizations, keeping a low system complexity.

This paper is organized as follows. Section II describes the automatic methodology to design the output combiner of the SLMBA. Section III evaluates and validates the proposed methodology in a practical SLMBA implementation. Moreover, a state-of-the-art comparison is made. Finally, conclusions are drawn in Section IV.

II. AUTOMATIC METHODOLOGY TO DESIGN THE SLMBA OUTPUT COMBINER

The objective of this section is to describe a PA design strategy requiring low human intervention and system complexity, while still performing competitively with the current state-of-the-art. Specifically, the methodology focuses on the design of the SLMBA output combiner, the key component on what the PA bandwidth is concerned.

The proposed methodology follows the algorithm presented in Fig. 4, in which its steps are described below.

1. Load-Pull Data Interpolation

The objective of this step is to build functions able to map discrete efficiency and output power values obtained from load-pull measurements or simulations to the load impedances presented to the active device. This function is shown in (1), $F\left(\Gamma_{L_{1H}}, \Gamma_{L_{2H}}\right)$:

$$\left[Eff_{\chi dB}, Pout_{\chi dB}\right] = F\left(\Gamma_{L_{1H}}, \Gamma_{L_{2H}}\right) \tag{1}$$

where $Eff_{\chi dB}$ and $Pout_{\chi dB}$ stand for the efficiency and output power, respectively, at χ dB compression, in which χ is defined by the PA designer.

Two similar extractions must be performed: for the balanced and control devices, according to their bias point, class C and class AB, respectively. Fundamental, $\Gamma_{L_{1H}}$, and second, $\Gamma_{L_{2H}}$, harmonic terminations were considered since they are the ones with direct impact on the device's efficiency and output power.

PA designers can change the inputs of (1) (e.g., add the second harmonic source termination) to the most appropriate according to the requirements and the device in use.

2. PAs Goals Setting

The desired goals for back-off and full power levels, and respective efficiency, should be defined at the selected compression point, for both balanced and control devices. For a reasonable goals specification, the output power and efficiency contours should be analyzed.

As previously described, for low power region only the CPA is active, which means that:

$$P_{out,SLMBA,BO} = P_{out,CPA,BO} \tag{2}$$

At full power region, the BPAs are on, thus the total SLMBA output power will be given by the sum of both BPAs and CPA generated powers:

$$P_{out,SLMBA,FP} = P_{out,CPA,FP} + 2 \cdot P_{out,BPA,FP} \tag{3}$$

After reach the triode region at the first back-off point, the CPA keeps its output power constant, i.e., $P_{out,CPA,BO} = P_{out,CPA,FP}$. Therefore, the CPA saturated power is determined by (4):

$$P_{out,CPA,FP} = \frac{P_{out,SLMBA,FP}}{OBO} \tag{4}$$

Replacing (4) in (3) we obtain:

$$P_{out,CPA,FP} = \frac{2}{OBO - 1} P_{out,BPA,FP} \tag{5}$$

Therefore, based on the desired OBO level and total SLMBA power it is possible to find the power ratio between the BPAs and CPA and therefore set the power levels goals for each device.

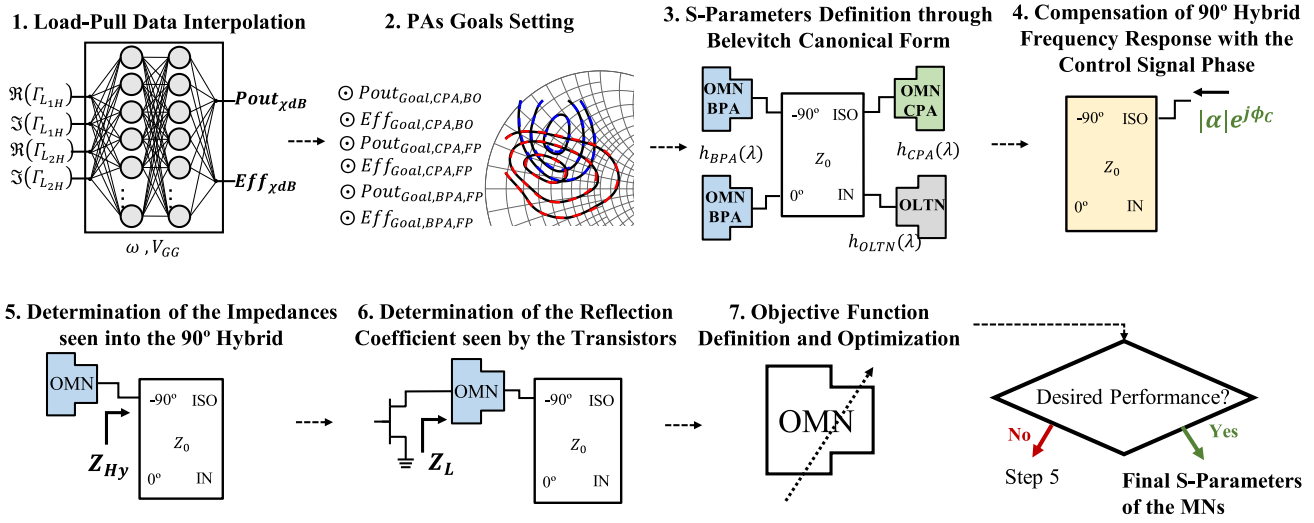

FIGURE 4. Flowchart of the proposed automatic algorithm.

3. S-Parameters Definition through the Belevitch Canonical Form

The matching networks connected to each port of the 90° hybrid, i.e., the PAs OMNs and the OLTN, shown in Fig. 1(a), should be described through S-parameter matrices, herein defined according to the well-known Belevitch canonical form. This form assumes that the S-parameters of a two-port network can be defined by a set of polynomials in the Richard's domain [30], as follows:

$$S = \begin{bmatrix} \dfrac{h(\lambda)}{g(\lambda)} & \dfrac{f(\lambda)}{g(\lambda)} \\ \dfrac{f(\lambda)}{g(\lambda)} & \dfrac{(-1)^{q+1}h(-\lambda)}{g(\lambda)} \end{bmatrix} \tag{6}$$

where $\lambda = jtan(\omega\tau)$, ω is the angular frequency and τ defines the length of the commensurate transmission lines [30]. $h(\lambda)$ and $f(\lambda)$ are polynomials defined for each MN following the forms of (7) and (8), respectively:

$$h(\lambda) = h_6\lambda^6 + h_5\lambda^5 + h_4\lambda^4 + h_3\lambda^3 + h_2\lambda^2 + h_1\lambda + h_0 \tag{7}$$

$$f(\lambda) = (-1)^q \lambda^q \left(1 - \lambda^2\right)^{N/2} \tag{8}$$

where the coefficients of $h(\lambda)$ are the optimization variables, q is the total number of zeros at dc and N the total number of cascaded sections. The $g(\lambda)$ polynomial is determined through the lossless condition [30].

Note that the reference impedances of the matching networks should also be defined. For simplicity, the PAs OMN reference impedance of port connected to the device should be close to the optimum impedance of the respective device. Likewise, the reference impedance of the port connected to the hybrid should be equal to the characteristic impedance of the hybrid.

The initial coefficients can be selected arbitrarily. However, for time-efficient reasons, the initial coefficients of the polynomials can be computed applying the simplified real frequency technique (SRFT) [30], using as goals the optimum power impedances. Naturally, for a wide frequency range, the selected profile will be non-Foster and the results from SRFT non-optimum. Nevertheless, it will be a decent starting point.

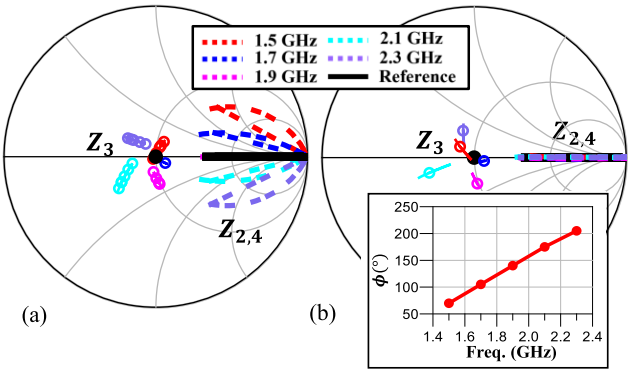

FIGURE 5. Impedance profiles at the hybrid reference plane with (a) constant ($\phi = 90°$) and (b) linearly variable phase, ϕ, represented versus frequency, of the control signal for ideal hybrid (solid black line) and for non-ideal hybrid (colored dashed lines) for different frequencies.

4. Compensation of 90° Hybrid Frequency Response with the Control PA Signal phase

As is common in all passive components based on quarter-wave transmission lines, a 90° hybrid is bandwidth limited. This means that the Z-parameters of such a pre-designed, or commercial, hybrid will noticeably depart from their idealized broadband values. Thus, for SLMBA design purposes, it is necessary to examine the hybrid frequency response when the current sources in Fig. 1 are directly injected into the hybrid.

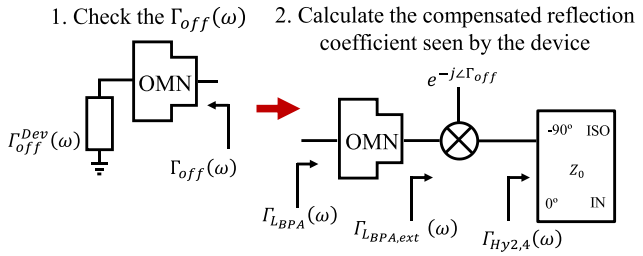

FIGURE 6. Process to obtain the compensated reflection coefficient seen by the balanced device.

The ideal load modulation, plotted in Fig. 5(a) in solid black, is obtained by applying the driving signals presented in Fig. 1, considering an ideal hybrid and an input phase control signal, ϕ_c, equal to 90°. As observed, and as can be verified through calculations, the ideal impedances at the hybrid reference planes are $Z_{Hy3} = Z_0$ and $Z_{Hy2,4} = Z_0(1+\sqrt{2}\alpha)$, which implies the desired optimum purely real load modulation of the BPAs.

Replacing the ideal hybrid with a non-ideal one (its design will be presented later on) and preserving the phase of the control signal, the results obtained from 1.5-2.3 GHz are presented in the colored lines of Fig. 5(a).

As observed, it is not possible to ensure a real load modulation for the whole frequency range and these obtained complex load trajectories are not desired as they will lead to SLMBA performance degradation.

However, in the SLMBA architecture, the phase of the control signal is a degree of freedom that we can explore. By adjusting ϕ_c for each frequency, so that the load modulation of the BPAs is purely real, it is possible to recover the performance in the balanced branch. Moreover, the ϕ_c variation is linear (see Fig. 5(b)), which means that it can be easily realized through a transmission line, allowing an implementation with a single analog input.

Unfortunately, since the isolation of the hybrid is not perfect across the entire bandwidth, when the power increases, a small variation of the impedance presented to the control PA is observed. Nevertheless, this variation can again be taken into account, and corrected, during the control OMN design.

5. Determination of the Impedances seen into the 90° Hybrid

The impedances seen into the hybrid can be computed as $Z_{Hy1...4} = V_{1...4}/I_{1...4}$, according with Fig. 1(a). Thus, based on the definition of I_2, I_3 and I_4, and on the Z-parameters of the pre-designed 90° hybrid, the voltages at the hybrid ports can be calculated.

Assuming that the Z-parameters of the hybrid and of the OLTN are represented, respectively, by $[Z]$ and $[Z_L]$, the I_1 can be computed as:

$$I_1 = \frac{(R_L + Z_{L22})\,(Z_{12}I_2 + Z_{13}I_3 + Z_{14}I_4)}{Z_{L12}Z_{L21} - (Z_L + Z_{L22})\,Z_{L11} - (Z_L + Z_{L22})\,Z_{11}} \quad (9)$$

being R_L the output load, usually 50 Ω.

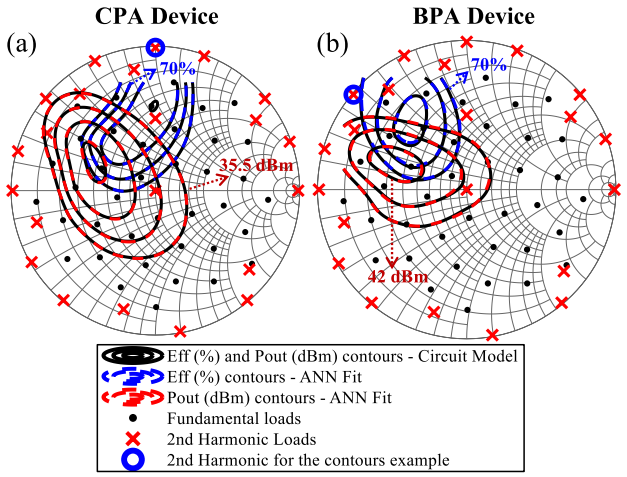

FIGURE 7. Comparison between efficiency and output power contours at 2 dB compression obtained from the circuit model and the extracted ANN models at 1.9 GHz for (a) the CPA and (b) the BPA devices referred to 50 Ω.

Naturally, $I_{2,4}$ and I_3 need to be set according to the power level, following Fig. 1(b). This means that, at back-off, $I_3 = \alpha_{FP} I_M$, being α_{FP} the maximum driving current normalized to the maximum BPAs current, I_M. $I_{2,4}$ are determined by taking into account the off-state impedance of the balanced devices (composed by the device's parasitic and OMN), the hybrid impedance matrix and (9).

In turn, at full power (i.e., $\beta = 1$ in Fig. 1), the currents will be given by $I_2 = I_M, I_3 = \alpha_{FP} I_M e^{j\phi_c}$ and $I_4 = jI_M$. Note that the input control phase, ϕ_c, is a vector of values that were adjusted according to the designed 90° hybrid (which is non-ideal), following the previous step of the algorithm.

After setting the currents, they are injected into the hybrid so that the port voltages can be calculated from its Z-parameters. Consequently, the impedances $Z_{Hy1...4}$ at back-off and full-power levels can be calculated and converted to reflection coefficients.

6. Determination of the Reflection Coefficient seen by the Transistors

The reflection coefficient seen by the CPA transistor, $\Gamma_{L_{CPA}}(\lambda)$, is computed using the S-parameters of the CPA OMN, defined in step 3, as follows:

$$\begin{aligned}\Gamma_{L_{CPA}}(\lambda) &= S_{11} + \frac{S_{12}S_{21}\Gamma_{Hy3}(\lambda)}{1 - S_{22}\Gamma_{Hy3}(\lambda)} \\ &= \frac{h_{CPA}(\lambda) + g_{CPA}(-\lambda)\,\Gamma_{Hy3}(\lambda)}{g_{CPA}(\lambda) + h_{CPA}(-\lambda)\,\Gamma_{Hy3}(\lambda)}\end{aligned} \quad (10)$$

where $\Gamma_{Hy3}(\lambda)$, is the reflection coefficient seen into the hybrid at port 3, i.e., the isolated port where the CPA is connected, (normalized to the hybrid's characteristic impedance, Z_0), obtained in step 5.

In order to mitigate the BPA off-state impedance problem described in [29], and, consequently, improve the SLMBA

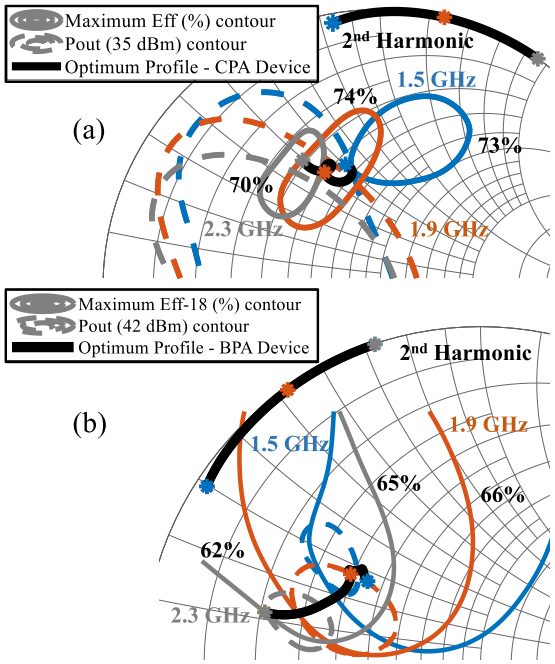

FIGURE 8. Efficiency (Eff) and output power (Pout) contours for three different frequencies, along with the optimum impedance profiles resulted from the proposed automatic method for the (a) CPA and (b) BPA device.

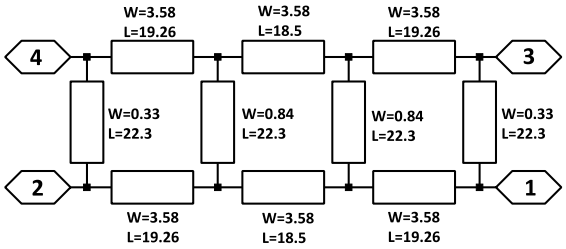

FIGURE 9. Schematic of the designed 90° hybrid. Length and width are in mm.

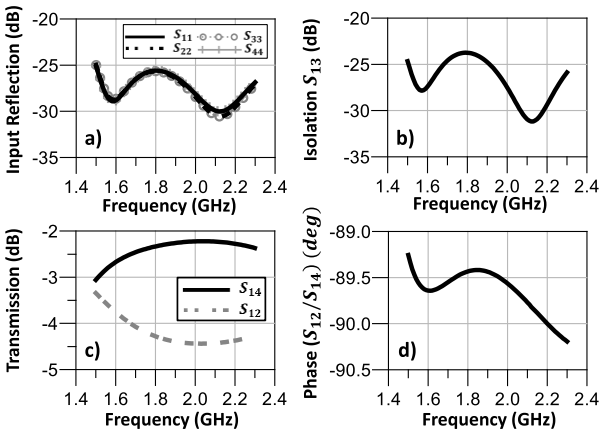

FIGURE 10. Electromagnetic scattering simulation results of the designed three-section branch line coupler.

bandwidth, the proposed design technique of [29] was incorporated in this automatic methodology.

Following [29], the reflection coefficient seen into the hybrid at ports 2 and 4 (i.e., the ones connected to the balanced branches), calculated in step 5, needs to be rotated according to the phase of the BPA off-state reflection coefficient.

The off-state reflection coefficient at the hybrid reference plane (taking into account the device extrinsic elements and the OMN), Γ_{off}, is computed as follows:

$$\Gamma_{off}(\lambda) = S_{22} + \frac{S_{12}S_{21}\Gamma_{off}^{Dev}}{1 - S_{22}} = \frac{g_{BPA}(-\lambda)\,\Gamma_{off}^{Dev} - h_{BPA}(-\lambda)}{g_{BPA}(\lambda) - h_{BPA}(\lambda)\,\Gamma_{off}^{Dev}} \tag{11}$$

in which Γ_{off}^{Dev} is the off-state reflection coefficient of the package device (not considering the OMN). Finally, the reflection coefficient seen by the BPA device is computed by (12). This process is illustrated in Fig. 6.

$$\Gamma_{L_{BPA}}(\lambda) = \frac{h_{BPA}(\lambda) + g_{BPA}(-\lambda)\,\Gamma_{Hy2,4}(\lambda)\,e^{-j\angle\Gamma_{off}}}{g_{BPA}(\lambda) + h_{BPA}(-\lambda)\,\Gamma_{Hy2,4}(\lambda)\,e^{-j\angle\Gamma_{off}}} \tag{12}$$

Therefore, (10) and (12) can be used as the inputs of (1), defined in step 1.

7. Objective Function Definition and Optimization

The objective function should be constructed so that the defined S-parameters can be incorporated into the inputs of (1), and the impedance profiles (10) and (12) can be optimized based on the defined performance metrics.

Thus, the objective function, $F_{obj}(.)$, is built as shown in (13), in which its inputs are computed using (10) and (12):

$$\begin{aligned} F_{obj} = \sum_{i=1}^{N} & \left(Pout_{Goal,CPA,BO} - F\left(\Gamma_{L1H,CPA}, \Gamma_{L2H,CPA}\right)\right)^2 \\ & + \left(Eff_{Goal,CPA,BO} - F\left(\Gamma_{L1H,CPA}, \Gamma_{L2H,CPA}\right)\right)^2 \\ & + \left(Pout_{Goal,CPA,FP} - F\left(\Gamma_{L1H,CPA}, \Gamma_{L2H,CPA}\right)\right)^2 \\ & + \left(Eff_{Goal,CPA,FP} - F\left(\Gamma_{L1H,CPA}, \Gamma_{L2H,CPA}\right)\right)^2 \\ & + \left(Pout_{Goal,BPA,FP} - F\left(\Gamma_{L1H,BPA}, \Gamma_{L2H,BPA}\right)\right)^2 \\ & + \left(Eff_{Goal,BPA,FP} - F\left(\Gamma_{L1H,BPA}, \Gamma_{L2H,BPA}\right)\right)^2 \\ & + \left(\left|\frac{h_{CPA}(2\lambda)}{g_{CPA}(2\lambda)}\right| - 1\right)^2 \\ & + \left(\left|\frac{h_{BPA}(2\lambda)}{g_{BPA}(2\lambda)}\right| - 1\right)^2 \end{aligned} \tag{13}$$

Note that we are forcing the S_{11} at the second harmonic of both the CPA and the BPA OMNs to be on the edge of the Smith chart. By definition of a lossless network, this means that S_{21} is zero, and thus $\Gamma_L(2\lambda) = S_{11} = \frac{h(2\lambda)}{g(2\lambda)}$, being this the second harmonic input of (1).

As previously mentioned, the CPA is connected to the isolated port, which means that, ideally, its output load is not modulated. However, as observed in Fig. 5, the hybrid isolation is not perfect and so the resulting load modulation profile will lead to a certain performance degradation. To mitigate the impedance variation, two goals were defined for the CPA, for back-off and full power levels. The BPAs goals are defined at full power. This means that the control PA OMN sets the back-off performance and both the CPA and the BPA OMNs contribute to the full power performance. Furthermore, note that there is no need to define any goal to design the OLTN. Since the voltages at the hybrid ports, and, consequently, the impedances $Z_{Hy1...4}$, depend on I_1, which, in turn, depends on the OLTN Z-parameters, make the above performance goals enough to optimize all the output combiner networks.

Although not represented in (13), for simplicity, it is possible to prioritize the goals represented in the objective function, by adding weights to each one. These weights are chosen by the PA designer, according to the requirements.

After achieving the desired performance, the proposed method outputs three S-parameters matrices in a polynomial form, representing the OMNs of the PAs and the OLTN. Finally, these S-parameters can then be synthesized, fitting them to a user-selected topology through microstrip lines and lumped elements.

III. METHODOLOGY EVALUATION, IMPLEMENTATION AND STATE-OF-ART COMPARISON

In this section the proposed automatic methodology is evaluated through a SLMBA output combiner design, in which the S-parameters of the OLTN and both OMNs of the CPA and BPAs are obtained, as described in the previous section.

The automatic method is assessed based on load-pull simulation data using real transistor models. This will allow us to have a better perception of the differences and advantages of the method without possible measurements error. Nevertheless, note that, if measured load-pull data is available, the nonlinear models are not required.

A. METHODOLOGY EVALUATION

In order to evaluate the proposed methodology, the output combiner of an SLMBA, presented in Fig. 1 (a), was designed using load-pull simulated data from nominal 6-W (CGH40006P) and 10-W (CGH40010F) GaN transistors for the CPA and BPAs, respectively.

The first step of the methodology was executed for both devices and for the frequency range of 1.5-2.3 GHz (42% of fractional bandwidth). The selected bias point for CPA and BPAs was respectively, $V_{GG} = -3.1V$ and $V_{DD} = 20V$ (class AB), and a $V_{GG} = -4.1V$ and $V_{DD} = 28V$ (class C), where V_{GG} stands for dc supply gate voltage and V_{DD} for dc supply drain voltage.

In order to map the efficiency and output power contours at 2 dB compression, (1) was built using an artificial neural network (ANN), using as inputs the fundamental and second harmonic terminations presented in Fig. 7 as black dots and red crosses, respectively. The comparison between efficiency and output power contours obtained from the circuit model and from the ANN models' extraction at 1.9 GHz is also presented in Fig. 7.

As observed, an ANN with only three layers of fifteen neurons proved enough to fit the data. Hyperbolic tangent functions were used as activation functions of the neurons, and the Bayesian Regularization algorithm was used to train the ANNs.

Although the BPA device is a nominal 10-W transistor, in practice, it is able to achieve 42 dBm, therefore, this value was used as full power goal for the BPAs. To accommodate high PAPR signals, the selected OBO was 10.5 dB, meaning that the SLMBA output power goals for back-off and full power were 35 dBm (CPA power level goals) and 45.5 dBm, respectively, according to (4) and (5). The efficiency goal was set to be the maximum possible (for the defined power levels) one for each frequency (by observing its contours – Fig. 8), which turned out to be 70% for both devices.

The CPA and BPA OMNs were defined through $h(\lambda)$ and $f(\lambda)$ polynomials according with (7) and (8), respectively, and setting $q = 0$. This was the selected form since it represents N consecutive transmission lines which corresponds to a universal topology [30]. For both CPA and BPA OMNs, a 6^{th} order network was selected, and for the OLTN a 4^{th} order network proved enough to provide the necessary real transformation.

A three-section branch line hybrid with $Z_0 = 30\Omega$ was selected to achieve the target bandwidth of 1.5-2.3 GHz. The hybrid schematic and its electromagnetic simulation are shown in Fig. 9 and Fig. 10, respectively. By performing step four of the methodology, the load-modulation at the hybrid reference plane was verified, being the profiles presented in Fig. 5(a). In order to ensure the purely real $Z_{Hy2,4}$ shown in Fig. 5(b), the phase of the control signal needs to follow the linear profile shown in the same figure.

After setting ϕ_c, the impedances seen into the hybrid and the respective reflection coefficient (normalized to Z_0) were computed following step five of the algorithm. Subsequently, the reflection coeffcients seen by the transistors were found (step six) and used as inputs of the objective function. Note that higher weights were applied to output power goals parcels in (13). That is because the objective is to strictly achieve the defined power levels with the highest possible efficiency for those levels.

After optimization, the obtained impedance profiles at fundamental and second harmonic, for the CPA and BPA devices are represented at solid black line in Fig. 8(a) and (b),

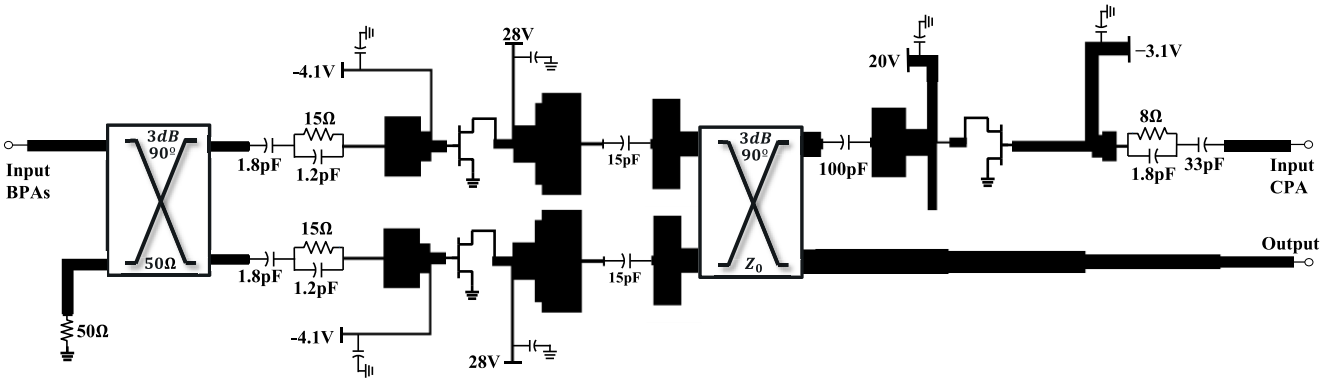

FIGURE 11. Simplified layout of the produced SLMBA.

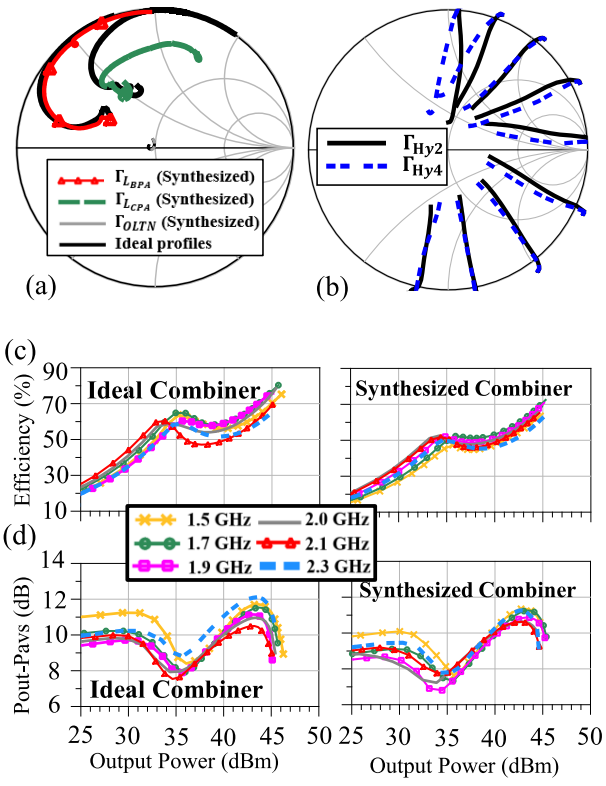

FIGURE 12. (a) Comparison between ideal and synthesized impedance profiles resulted from the methodology and (b) simulated load modulation of the BPAs at the hybrid reference plane. Drain efficiency (c) and added power (Pout-Pavs) (d) versus output power with the ideal and synthesized combiner.

respectively. Moreover, to evaluate if the obtained profile is, in fact, optimum, and how it compares with the defined goals, the efficiency and output power contours, for the obtained second harmonic, were plotted.

As can be observed through Fig. 8, besides the obtained impedance profiles require less time and human intervention, they also attained nearly the desired power levels and efficiency goal (except for the BPA at 2.3 GHz) demonstrating a good performance of the proposed automatic methodology.

B. IMPLEMENTATION AND MEASUREMENTS

The optimum $h(\lambda)$ polynomials for each matching network are presented in (14), by which their S-parameters were extracted through (6). Microstrip lines and lumped capacitors were then used to synthesize the obtained profiles, already including the necessary bias network and dc-block capacitor.

$$\begin{cases} h_{BPA}(\lambda) = 45.8\lambda^6 + 68.5\lambda^5 + 198\lambda^4 - 137\lambda^3 \\ -7.2\lambda^2 - 8.8\lambda - 0.26 \\ h_{CPA}(\lambda) = 2470\lambda^6 - 167\lambda^5 + 435\lambda^4 - 96\lambda^3 \\ +9.3\lambda^2 - 7.4\lambda - 0.26 \\ h_{OLTN}(\lambda) = -0.02\lambda^4 - 0.25\lambda^3 - 0.02\lambda^2 \\ -0.6\lambda - 0.26 \end{cases} \tag{14}$$

The IMNs of both PAs were designed to provide enough gain without compromising efficiency in the selected bandwidth. Moreover, to ensure the SLMBA stabilization, a parallel RC circuit was placed at the input of each amplifier, and a resistor at each gate was also required.

To simplify the design, the SLMBA was implemented with two digital inputs (for the BPAs and CPA), as observed in the layout presented in Fig. 11, built on 20-mil thick Rogers 4350B substrate with dielectric constant of 3.48. For that, another 90° hybrid was incorporated to split the signal to the BPAs.

Fig. 12(a) presents the comparison between the ideal impedance profiles resulted directly from the method, with the ones resulted from their synthesis with microstrip lines and lumped elements. Furthermore, in Fig. 12(c) and (d) it is respectively plotted the simulated drain efficiency and added power (difference between output power and power provided to the CPA and BPAs, P_{avs}) versus output power of both scenarios. Note that, since digital control is used, the gain of the PA is inherently linear, since for each power level the input driving signals are selected to provide the desired output power level. Additionally, these signals excitations are also

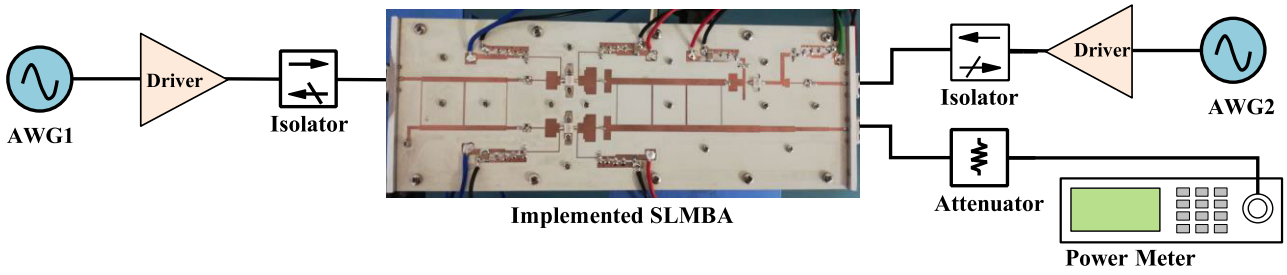

FIGURE 13. Measurement setup (DC power supply was omitted) and implemented SLMBA.

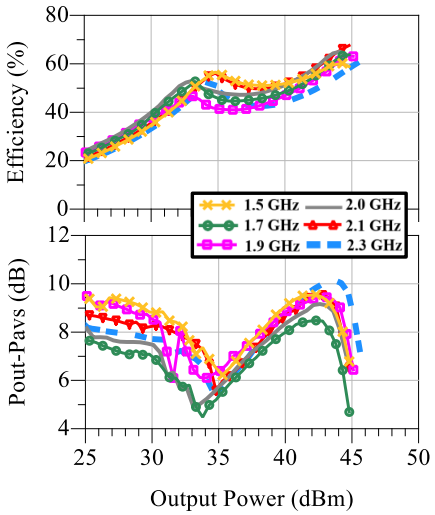

FIGURE 14. Measured drain efficiency and added power versus output power for several frequencies.

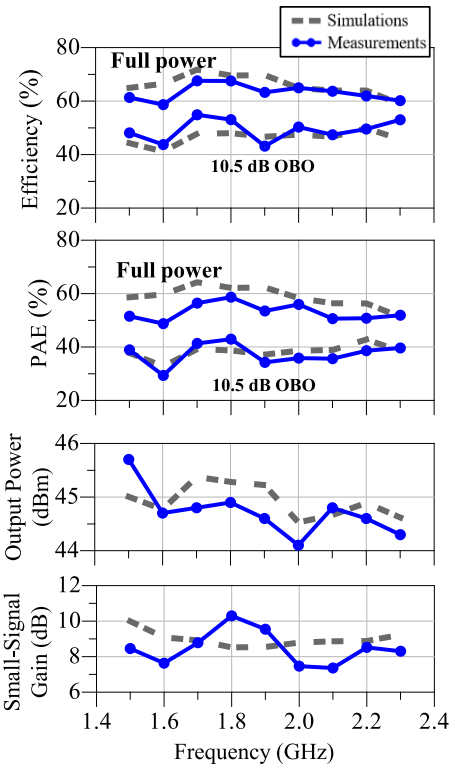

FIGURE 15. Simulated and measured efficiency and PAE at 0 and 10.5 dB, output power at full power and small-signal gain over frequency.

selected for optimized efficiency. The plotted added power only reveals how much power was required in both channels to obtain the desired power.

As can be observed, although there is an efficiency decrease with the synthesized combiner – due to losses and also some imprecision when fitting the control impedance profile –, the desired power levels for the efficiency peaks are in accordance with the ideal combiner and with the desired goals: 35 dBm and 45.5 dBm. A good agreement between the optimum and the synthesized impedance profiles of the balanced OMN and the OLTN was attained, making the full power level and respective efficiency similar to the ideal one.

The load modulation of the BPAs at the hybrid plane, $\Gamma_{Hy2,4}$ is also showed in Fig. 12(b). The almost straight load modulation observed, along with a decent efficiency performance between the two peaks (full power and 10.5 dB OBO), verifies that the off-state impedance of the BPAs is compensated [29].

The implemented PA was measured under pulsed CW excitation for experimental validation over the operating frequency range. The signals were generated with an arbitrary waveform generator (AWG) and the output power was measured using a power meter. Two broadband linear drivers were used to provide enough input power to the SLMBA. The measurement setup is shown in Fig. 13, along with the implemented SLMBA (24.9 × 9.2 cm).

The measured drain efficiency and added power versus output power is plotted in Fig. 14.

In Fig. 15, the comparison between the simulated and measured drain efficiency and PAE for OBO and full power levels, over frequency, is presented. Moreover, the maximum output power and small-signal gain (which corresponds to the first point of the added power data of Fig. 12(d)) versus frequency is also depicted in the same figure.

Observing Fig. 15 and comparing Fig. 14 with Fig. 12(c) and (d), it can be concluded that there is a good agreement between simulations and measurements. It can

TABLE 1. Performance comparison of recently published load modulated balanced amplifiers.

Ref. /Year	Architecture	Freq. (GHz)	FBW (%)	P_{Max} (dBm)	$E_{ff}@P_{Max}$ (%)	$E_{ff}@OPBO$ (%)	$OPBO$ (dB)
[13] / 2017	RF-Input LMBA	1.8-3.8	71	44	46-70	33-49	6
[14] / 2018	Dual-Input LMBA	1.7-2.5	38	48-48.9	48-58*	39-50*	8
[15] / 2020	RF-Input CM-LMBA	1.45-2.45	51.3	45.6-46.7	67.1-77.9	47.8-55.7	8
[16] / 2020	RF-Input SLMBA	3.05-3.55	15	42.3-43.7	60.8-74.8	43.2-51.4	10
[17] / 2020	RF-Input PD-LMBA	1.5-2.7	57	42.5	58-72	47-58	10
[19] / 2021	RF-Input PD-ALMBA	0.55-2.2	120	41-43	49-82	39-64	10
[20] / 2022	RF-Input W-SLMBA	1.8-2.75	41.8	44.6-45.8	60.2-68.3	51.8-69	8
This Work	Dual-Input SLMBA	1.5-2.3	42	44-45.7	59-68 (49-59)*	43-55 (30-43)*	10.5

*Power Added Efficiency (PAE)

also be observed that there is a difference between the drain efficiency and the PAE, which indicates that the PA design was not properly optimized for gain, as can be also observed in the small signal gain graphic. The final SLMBA attained a measured peak output power of 44-45.7 dBm with a drain efficiency of 59-68% and 43-55% at 10.5dB of OBO (from the measured peak output power), for 1.5-2.3 GHz.

C. STATE-OF-THE-ART COMPARISON

Table 1 summarizes the performance comparison between this design and other recently reported LMBAs with similar frequency range and output power.

In [13] the optimum impedance selection is made manually, through load-pull. Alternatively, [14], [15], [16], [17], [19], and [20] do the analysis at the intrinsic reference plane and then, by nonlinear embedding of the (required to be known) package parasitics, the frequency dependent impedance at the package reference plane is found. After selecting the optimum profiles, the referred works use optimization tools to approximate those profiles. All these techniques, suffer from the aforementioned issues, requiring a significant expertise and experience from the PA designer to select proper impedance profiles that can be synthetized with a passive matching network, without losing performance in the end.

In comparison, the proposed design does not require an open device model, being able to operate directly with load-pull data (simulated or measured) and minimizing the error directly over the desired performance – output power and efficiency. Furthermore, since it uses an automatic method to search for the optimum profiles, it requires much less human intervention, and possible tuning in the lab.

In performance terms and focusing our analysis in [16], [17], and [19] where the OBO is the similar to our design, it is observed that: the proposed design can achieve higher FBW and output power than [16], while obtaining less (about 7%) efficiency at full power, but a higher one (about 4%) at back-off. In [17] a higher FBW and efficiency (mainly at back-off) is obtained when compared to our work. Nevertheless, a higher output power (more than 1.5 dB) is obtained in our work, which may indicate that the efficiency and bandwidth were sacrificed in return. In [19], although a much higher FBW is obtained, the output power is at least 1 dB lower than our proposed design, and the efficiency varies significantly, reaching higher upper values, but also smaller lower values, than our results.

Based on this analysis we conclude that, besides our design does not require a nonlinear device model and has less human intervention, its performance is still competitive with the current state-of-the-art.

IV. CONCLUSION

In this paper, an automatic SLMBA design that considers the non-ideal frequency response of the 90° hybrid, used as the output combiner, is proposed. Based on the active devices' load-pull data and on the dependency of the 90° hybrid on frequency, the method directly optimizes the matching network S-parameters, that compose the output combiner, to achieve the desired output power and efficiency, taking into account the optimum CPA phase response and the BPAs' off-state impedance. Thus, minimizing the human intervention in the impedance selection and its inherent constraints. By realizing the obtained S-parameters through physical networks, a 42% FBW SLMBA was produced

and measured, validating the proposed method. Finally, the design method and the obtained performance was compared with the most recent published broadband LMBAs. In additon to not requiring a nonlinear model for the device and to have less human intervention in the impedance profile selection, the proposed design demonstrated to perform competitively with other state-of-the-art previous works.

REFERENCES

[1] W. H. Doherty, "A new high efficiency power amplifier for modulated waves," *Proc. Inst. Radio Eng.*, vol. 24, no. 9, pp. 1163–1182, Sep. 1936.
[2] V. Camarchia, M. Pirola, R. Quaglia, S. Jee, Y. Cho, and B. Kim, "The Doherty power amplifier: Review of recent solutions and trends," *IEEE Trans. Microw. Theory Techn.*, vol. 63, no. 2, pp. 559–571, Feb. 2015.
[3] M. Özen, K. Andersson, and C. Fager, "Symmetrical Doherty power amplifier with extended efficiency range," *IEEE Trans. Microw. Theory Techn.*, vol. 64, no. 4, pp. 1273–1284, Apr. 2016.
[4] W. Hallberg, M. Özen, D. Gustafsson, K. Buisman, and C. Fager, "A Doherty power amplifier design method for improved efficiency and linearity," *IEEE Trans. Microw. Theory Techn.*, vol. 64, no. 12, pp. 4491–4504, Dec. 2016.
[5] J. Kim, "2.4 GHz class-F^{-1} GaN Doherty amplifier with efficiency enhancement technique," *IEEE Microw. Wireless Compon. Lett.*, vol. 28, no. 1, pp. 34–36, Jan. 2018.
[6] Y. Xu, J. Pang, X. Wang, and A. Zhu, "Enhancing bandwidth and back-off range of Doherty power amplifier with modified load modulation network," *IEEE Trans. Microw. Theory Techn.*, vol. 69, no. 4, pp. 2291–2303, Apr. 2021.
[7] H. Chireix, "High power outphasing modulation," *Proc. Inst. Radio Eng.*, vol. 23, no. 11, pp. 1370–1392, Nov. 1935.
[8] T. W. Barton and D. J. Perreault, "Theory and implementation of RF-input outphasing power amplification," *IEEE Trans. Microw. Theory Techn.*, vol. 63, no. 12, pp. 4273–4283, Dec. 2015.
[9] M. Özen, M. van der Heijden, M. Acar, R. Jos, and C. Fager, "A generalized combiner synthesis technique for class-E outphasing transmitters," *IEEE Trans. Circuits Syst. I, Reg. Papers*, vol. 64, no. 5, pp. 1126–1139, May 2017.
[10] L. C. Nunes, F. M. Barradas, D. R. Barros, P. M. Cabral, and J. C. Pedro, "Current mode outphasing power amplifier," in *IEEE MTT-S Int. Microw. Symp. Dig.*, Jun. 2019, pp. 1160–1163.
[11] C. Liang, J. I. Martinez-Lopez, P. Roblin, Y. Hahn, D. Mikrut, and V. Chen, "Wideband two-way hybrid Doherty outphasing power amplifier," *IEEE Trans. Microw. Theory Techn.*, vol. 69, no. 2, pp. 1415–1428, Feb. 2021.
[12] D. J. Shepphard, J. Powell, and S. C. Cripps, "An efficient broadband reconfigurable power amplifier using active load modulation," *IEEE Microw. Wireless Compon. Lett.*, vol. 26, no. 6, pp. 443–445, Jun. 2016.
[13] P. H. Pednekar, E. Berry, and T. W. Barton, "RF-input load modulated balanced amplifier with octave bandwidth," *IEEE Trans. Microw. Theory Techn.*, vol. 65, no. 12, pp. 5181–5191, Dec. 2017.
[14] R. Quaglia and S. Cripps, "A load modulated balanced amplifier for telecom applications," *IEEE Trans. Microw. Theory Techn.*, vol. 66, no. 3, pp. 1328–1338, Mar. 2018.
[15] J. Pang, C. Chu, Y. Li, and A. Zhu, "Broadband RF-input continuous-mode load-modulated balanced power amplifier with input phase adjustment," *IEEE Trans. Microw. Theory Techn.*, vol. 68, no. 10, pp. 4466–4478, Oct. 2020.
[16] J. Pang, Y. Li, M. Li, Y. Zhang, X. Y. Zhou, Z. Dai, and A. Zhu, "Analysis and design of highly efficient wideband RF-input sequential load modulated balanced power amplifier," *IEEE Trans. Microw. Theory Techn.*, vol. 68, no. 5, pp. 1741–1753, May 2020.
[17] Y. Cao and K. Chen, "Pseudo-Doherty load-modulated balanced amplifier with wide bandwidth and extended power back-off range," *IEEE Trans. Microw. Theory Techn.*, vol. 68, no. 7, pp. 3172–3183, Jul. 2020.
[18] K. Chaudhry, R. Quaglia, and S. Cripps, "A load modulated balanced amplifier with linear gain response and wide high-efficiency output power back-off region," in *Proc. Int. Workshop Integr. Nonlinear Microw. Millim.-Wave Circuits (INMMiC)*, Jul. 2020, pp. 1–3.
[19] Y. Cao, H. Lyu, and K. Chen, "Asymmetrical load modulated balanced amplifier with continuum of modulation ratio and dual-octave bandwidth," *IEEE Trans. Microw. Theory Techn.*, vol. 69, no. 1, pp. 682–696, Jan. 2021.
[20] C. Chu, T. Sharma, S. K. Dhar, R. Darraji, X. Wang, J. Pang, and A. Zhu, "Waveform engineered sequential load modulated balanced amplifier with continuous class-F^{-1} and class-J operation," *IEEE Trans. Microw. Theory Techn.*, vol. 70, no. 2, pp. 1269–1283, Feb. 2022.
[21] C. Belchior, L. C. Nunes, P. M. Cabral, and J. C. Pedro, "Automatic methodology for wideband power amplifier design," *IEEE Microw. Wireless Compon. Lett.*, vol. 31, no. 8, pp. 989–992, Aug. 2021.
[22] C. Liang, P. Roblin, Y. Hahn, and Y. Xiao, "Automatic algorithm for the direct design of asymmetric Doherty power amplifiers," in *Proc. IEEE Top. Conf. RF/Microw. Power Modeling Radio Wireless Appl. (PAWR)*, Jan. 2019, pp. 1–4.
[23] C. Liang, P. Roblin, and Y. Hahn, "Accelerated design methodology for dual-input Doherty power amplifiers," *IEEE Trans. Microw. Theory Techn.*, vol. 67, no. 10, pp. 3983–3995, Oct. 2019.
[24] P. Chen, B. M. Merrick, and T. J. Brazil, "Bayesian optimization for broadband high-efficiency power amplifier designs," *IEEE Trans. Microw. Theory Techn.*, vol. 63, no. 12, pp. 4263–4272, Dec. 2015.
[25] P. Chen, J. Xia, B. M. Merrick, and T. J. Brazil, "Multiobjective Bayesian optimization for active load modulation in a broadband 20-W GaN Doherty power amplifier design," *IEEE Trans. Microw. Theory Techn.*, vol. 65, no. 3, pp. 860–871, Mar. 2017.
[26] C. Li, F. You, T. Yao, J. Wang, W. Shi, J. Peng, and S. He, "Simulated annealing particle swarm optimization for high-efficiency power amplifier design," *IEEE Trans. Microw. Theory Techn.*, vol. 69, no. 5, pp. 2494–2505, May 2021.
[27] H. Liu, C. Li, S. He, W. Shi, Y. Chen, and W. Shi, "Simulated annealing particle swarm optimization for a dual-input broadband GaN Doherty like load-modulated balance amplifier design," *IEEE Trans. Circuits Syst. II, Exp. Briefs*, vol. 69, no. 9, pp. 3734–3738, Sep. 2022.
[28] C. Belchior, L. C. Nunes, P. M. Cabral, and J. C. Pedro, "Output impedance profile selection in sequential LMBAs using an automatic method," in *Proc. Int. Workshop Integr. Nonlinear Microw. Millim.-Wave Circuits (INMMiC)*, Apr. 2022, pp. 1–3.
[29] C. Belchior, L. C. Nunes, P. M. Cabral, and J. C. Pedro, "Sequential LMBA design technique for improved bandwidth considering the balanced amplifiers off-state impedance," *IEEE Trans. Microw. Theory Techn.*, early access, Feb. 17, 2023, doi: 10.1109/TMTT.2023.3241690.
[30] S. Yarman, *Design of Ultra Wideband Power Transfer Networks*. New York, NY, USA: Wiley, 2010.

CATARINA BELCHIOR (Graduate Student Member, IEEE) was born in Açores, Portugal, in July 1996. She received the M.Sc. degree in electronic and telecommunications engineering from Universidade de Aveiro, Portugal, in 2019, where she is currently pursuing the Ph.D. degree in electrical engineering. She has been with the Institute of Telecommunications, Aveiro, Portugal, as a Junior Researcher, since 2016. Her research interests include active device modeling and automatic PA design methodologies for wideband operation. She is a Student Member of the IEEE Microwave Theory and Techniques Society (IEEE MTT-S) and a member of the IEEE MTT-S Student Branch Chapter with Universidade de Aveiro.

LUÍS C. NUNES (Member, IEEE) was born in Guarda, Portugal, in October 1986. He received the M.Sc. and Ph.D. degrees in electrical engineering from Universidade de Aveiro, Portugal, in 2010 and 2015, respectively. From 2016 to 2017, he was a RF Design Engineer with Huawei Technologies, Sweden. He is currently a Researcher Assistant with the Institute of Telecommunications, Aveiro, Portugal. His research interests include active device modeling, nonlinear distortion analysis, and the design of microwave circuits, especially high-efficiency and linear power amplifiers. He is a member of the IEEE Microwave Theory and Techniques Society (IEEE MTT-S) and the IEEE Electron Devices Society.

PEDRO M. CABRAL (Senior Member, IEEE) was born in Portugal, in October 1979. He received the degree in electrical engineering and the Ph.D. degree from Universidade de Aveiro, Aveiro, Portugal, in 2002 and 2006, respectively. He is currently a Senior Researcher with Instituto de Telecomunicações, Aveiro, and an Assistant Professor with Universidade de Aveiro. His current research interests include active device nonlinear modeling, the design of microwave circuits, high-efficiency PAs, and wireless transmitter architectures. He has been a Reviewer of several publications, including the IEEE TRANSACTIONS ON MICROWAVE THEORY AND TECHNIQUES, the IEEE TRANSACTIONS ON COMPUTER-AIDED DESIGN OF INTEGRATED CIRCUITS AND SYSTEMS, the IEEE TRANSACTIONS ON INSTRUMENTATION AND MEASUREMENT, and the IEEE TRANSACTIONS ON CIRCUITS AND SYSTEMS—I: REGULAR PAPERS.

JOSÉ C. PEDRO (Fellow, IEEE) received the Diploma, Ph.D., and Habilitation degrees in electronics and telecommunications engineering from Universidade de Aveiro, Aveiro, Portugal, in 1985, 1993, and 2002, respectively.

He is currently a Full Professor with Universidade de Aveiro and the President of Instituto de Telecomunicações. He has authored two books and authored or coauthored more than 200 papers in international journals and symposia. His current research interests include active device modeling and the analysis and design of various nonlinear microwave circuits.

Dr. Pedro was a recipient of various prizes including the 1993 Marconi Young Scientist Award, the 2000 Institution of Electrical Engineers Measurement Prize, the 2015 EuMC Best Paper Microwave Prize, and the Microwave Distinguished Educator Award. He has served the scientific community as a Reviewer and an Editor for several conferences and journals, namely, the IEEE TRANSACTIONS ON MICROWAVE THEORY AND TECHNIQUES, for which he was the Editor-in-Chief.